THE JOURNAL OF PHYSICAL CHEMISTRY C

ARTICLE

pubs.acs.org/JPCC

Effect of the Methanol-to-Olefin Conversion on the PFG NMR Self-Diffusivities of Ethane and Ethene in Large-Crystalline SAPO-34

Weili Dai,[†,‡] Matthias Scheibe,[‡] Landong Li,[*,†] Naijia Guan,[†] and Michael Hunger[*,‡]

[†]Key Laboratory of Advanced Energy Materials Chemistry (Ministry of Education), College of Chemistry, Nankai University, Tianjin 300071, P. R. China

[‡]Institute of Chemical Technology, University of Stuttgart, 70550 Stuttgart, Germany

ABSTRACT: SAPO-34 catalysts obtained after MTO conversion times of 0−30 min were investigated by PFG NMR spectroscopy for studying the self-diffusivities of ethane and ethene. Furthermore, the catalysts were investigated by in situ UV/vis, ^{13}C MAS NMR, and ^{1}H MAS NMR spectroscopy, giving insights into the organic deposits and acid sites in different periods of the catalyst lifetime. The ratio of the self-diffusivities of ethene and ethane, D_{ethene}/D_{ethane}, used as a measure of the diffusion selectivity, was found to increase to the benefit of the olefin compared to the alkane for higher adsorbate loadings and increasing MTO conversion times. This change of the diffusion selectivity is one of the reasons for the variation of the product selectivity during the catalyst lifetime. Variable-temperature PFG NMR studies gave a significantly larger apparent activation energy for the self-diffusivity of ethane (E_a = 7.6 kJ/mol) compared with ethene (E_a = 4.2 kJ/mol).

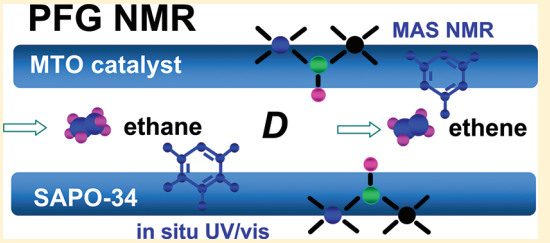

1. INTRODUCTION

The rapid increase in the price of crude oil and the increasing demands on light olefins require the search for new routes for the production of hydrocarbons from non-oil sources, such as natural gas and coal. Among these alternative reaction routes, the methanol-to-olefin (MTO) conversion on microporous solid acids is an important step drawing more and more attention in the past years.[1,2] In the MTO process, methanol is dehydrated to dimethyl ether (DME), and an equilibrium mixture consisting of methanol, DME, and water is obtained, which is the feed for the conversion to light olefins over acidic microporous catalysts, such as aluminosilicate- and silicoaluminophosphate-type zeolites (e.g., ZSM-5 and SAPO-34, respectively). According to an often-discussed reaction mechanism, formation of first organic compounds occurs during an induction period, leading to a hydrocarbon pool consisting of large olefins and/or alkylaromatics inside the catalyst pores or cages. The reactants methanol and DME are repeatedly added to these hydrocarbon pool compounds, while light olefins are split off in a closed cycle.[3,4] The distribution of reaction products depends on a number of parameters, such as density and strength of Brønsted acid sites, diameters and shapes of micropores and cages, and type of resistant organic deposits being the catalytically active hydrocarbon pool compounds. As for many heterogeneously catalyzed reactions, therefore, the pore diffusion of reactants can strongly affect the reaction kinetics and shape selectivity of the MTO reaction.[5,6]

A variety of microporous catalysts with different acidities and pore architectures have been studied as MTO catalysts.[1,2,7,8] The silicoaluminophosphate SAPO-34 with CHA structure consisting of large chabazite cages with 8-ring windows and characterized by Brønsted acid sites of moderate acid strength is reported to be a most promising catalyst giving yields of light olefins (mainly ethene and propene) of up to 80%.[9] The mechanistic aspects of the MTO reaction on SAPO-34 have been extensively studied,[9−17] and it is indicated that polyalkylaromatics are confined inside the chabazite cages of SAPO-34 (diameter of ca. 0.94 nm). They are the active hydrocarbon pool compounds leading to the formation of light olefins.[13] The 8-ring windows with a diameter of ca. 0.38 nm restrict the diffusion of large and branched hydrocarbons and, therefore, influence the selectivity to the reaction products. Furthermore, the Brønsted sites of SAPO-34, formed via substituting lattice phosphorus by silicon atoms, are characterized by a moderate acid strength. This property results in better resistance to coking and, therefore, causes a longer catalyst lifetime in the MTO reaction in comparison with the aluminosilicate analogue SSZ-13.[17]

In the present study, the relationship of organic deposits, acid site density, diffusion properties, and catalytic activity of SAPO-34 in the MTO conversion has been investigated. The dependence of the methanol conversion and product selectivity on the Brønsted acid sites and organic deposits was already investigated in our recent studies.[18,19] For the investigation of the adsorbate diffusion in microporous materials, IR spectroscopic techniques,[20] quasi-elastic neutron scattering,[21] and dielectric spectroscopy[22] are successfully utilized. Pulsed-field gradient NMR spectroscopy (PFG NMR) is suitable for determining the intracrystalline self-diffusivity, D, of small hydrocarbons.[23,24] With this method, the effect of molecular self-diffusion on the signal

Received: September 13, 2011
Revised: December 19, 2011
Published: December 22, 2011

   dx.doi.org/10.1021/jp208815g | J. Phys. Chem. C 2012, 116, 2469–2476

attenuation of NMR echo experiments as a function of the duration or strength of pulsed magnetic field gradients is evaluated.[23,24]

To the best of our knowledge, there are only very few PFG NMR self-diffusion studies of adsorbates in CHA-type zeolites.[25,26] According to Hedin et al.,[26] ethane and ethene give PFG NMR self-diffusivities of $D = 0.48 \times 10^{-12}$ m^2/s and $D = 3.1 \times 10^{-12}$ m^2/s, respectively, in pure siliceous chabazite (Si-CHA) upon loading with an adsorbate pressure of $p = 101.2$ Pa and at the temperature of $T = 301$ K. Assuming that the PFG NMR self-diffusivity of ethene in SAPO-34 is in the order of $D \approx 10^{-12}$ m^2/s and using an observation time of $\Delta \approx 40$ ms, which is the experimental diffusion time, the Einstein equation[27]

$$D = \langle x \rangle^2 / 6\Delta \quad (1)$$

allows to estimate the molecular displacement x of up to 0.5 μm for the above-mentioned molecule. For studying pure intracrystalline self-diffusion of ethane and ethene, therefore, the size of zeolite crystals utilized for PFG NMR experiments have to be significantly larger than 0.5 μm. Therefore, the synthesis of large-crystalline SAPO-34 was an important prerequisite for the present PFG NMR study. Furthermore, application of a large-crystalline SAPO-34 material as catalyst for the MTO conversion gives an insight into the influence of the crystal size on the catalyst property and lifetime.

2. EXPERIMENTAL SECTION

2.1. Preparation and Characterization of the Catalyst. Large-crystalline SAPO-34 with the $n_{Si}/(n_{Al} + n_P + n_{Si})$ ratio of 0.15 was synthesized by the hydrothermal method following the procedure described in the literature.[28] The molar composition for synthesis was kept at 1.0 Al_2O_3:1.0 P_2O_5:0.6 SiO_2:2.0 Mor:60 H_2O. Orthophosphoric acid solution (85 wt %) and aluminum triisopropylate (ATI) were mixed with distilled water and stirred for 2 h, followed by addition of morpholine (Mor) and silica sol (30 wt % VPAC4083) dropwise. Then, the mixture was stirred at room temperature for 6 h. Thereafter, the formed gel was transferred into a Teflon-lined stainless steel autoclave and crystallized at 463 K for 48 h. The solid product was washed four times with demineralized water and separated by a centrifuge, followed by drying at 353 K for 12 h. The as-synthesized sample was then calcined in flowing synthetic air at 873 K for 4 h.

X-ray diffraction (XRD) patterns of the as-synthesized and calcined samples were recorded on a Bruker D8 diffractometer with Cu Kα radiation ($\lambda = 1.5418$ Å) at 5°−50° with a scan speed of $2\theta = 6.0°$/min.

A Hitachi S-4700 scanning electron microscope (SEM) was used for studying the crystal morphologies of the sample. The SEM image was recorded after covering the sample with a thin layer of gold, deposited by sputtering.

The chemical composition of the calcined sample was determined by ICP-OES. The surface area of the calcined SAPO-34 was obtained by means of nitrogen adsorption at 77 K on a Quantachrome Autosorb 3B instrument. Before the nitrogen adsorption, the sample was dehydrated at 473 K for 2 h. The total surface area was calculated via the Brunauer−Emmett−Teller (BET) equation.

2.2. Catalytic Investigations and Characterization of Occluded Organic Compounds on the MTO Catalysts. The MTO reaction was performed in a fixed-bed reactor at atmospheric pressure and the reaction temperature of 643 K. Typically, 0.4 g of sample (sieve fraction, 0.25−0.5 mm) was placed in a stainless steel reactor (5 mm i.d.) and activated under flowing nitrogen at 723 K for 2 h. A methanol flow of 0.5 mL/h corresponding to a weight hourly space velocity of WHSV = 1 h^{-1} was used. The reaction products were analyzed using an online gas chromatograph equipped with a flame ionization detector and a capillary column Plot Q to separate C_1−C_8 hydrocarbons. At first, the temperature of the column was maintained at 313 K for 15 min and then increased to 473 K with a rate of 10 K/min. For detailed investigations of the nature of the organic deposits, the fate of Brønsted acid sites, and the diffusion properties of adsorbates in large-crystalline SAPO-34 used as MTO catalyst, samples were taken from the fixed-bed reactor after times on stream of TOS = 5 min (sample B), 10 min (sample C), and 30 min (sample D). Sample A is the calcined SAPO-34 material, which is obtained before starting the MTO conversion (TOS = 0 min).

The organic compounds formed on the MTO catalysts during the methanol conversion were investigated by in situ UV/vis spectroscopy using a fiber-optic UV/vis spectrometer. UV/vis spectra in the range of 200−600 nm in diffuse reflection mode were recorded with an AvaSpec-2048 fiber-optic spectrometer using an AvaLight-DH-S deuterium light source by Avantes and a glass fiber reflection probe HPSUV1000A by Oxford Electronics. Reference UV/vis spectra of the silicoaluminophosphate were recorded at reaction temperature prior to starting the methanol conversion. The amounts of occluded hydrocarbons after the methanol reaction were analyzed by thermogravimetric analysis (TGA) on a SETARAM Setsys 16/18 analyzer. In a typical measurement, 0.1 g of the sample material was heated in an Al_2O_3 crucible with a constant heating rate of 10 K/min and under flowing synthetic air (30 mL/min).

The organic deposits occluded inside the pores and cages of the MTO catalysts were characterized by ^{13}C MAS NMR spectroscopy utilizing a Bruker Avance III 400WB spectrometer at the resonance frequency of 100.6 MHz, with $\pi/2$ pulse excitation and high-power proton decoupling, the repetition time of 20 s, and using a 4 mm MAS NMR probe with the sample spinning rate of 12.0 kHz. To avoid contact with air, all catalyst samples studied by NMR spectroscopy were transferred into gastight MAS NMR rotors or glass tubes in a glovebox purged with dry nitrogen gas.

2.3. Solid-State NMR Characterization of Surface Sites and Pulsed-Field Gradient (PFG) NMR Self-Diffusion Studies. The Brønsted acid sites of the samples were characterized by means of ^{1}H MAS NMR spectroscopy utilizing a Bruker Avance III 400WB spectrometer at the resonance frequency of 400.1 MHz, with $\pi/2$ single pulse excitation, the repetition time of 10 s, and using 4 mm MAS NMR probes with a sample spinning rate of 8.0 kHz. The samples studied by ^{1}H MAS NMR spectroscopy were dehydrated at 673 K in vacuum (pressure below 10^{-2} Pa) for 12 h. After dehydration, the samples were sealed and kept in glass tubes until they were transferred into MAS NMR rotors inside a glovebox purged with dry nitrogen gas. The determination of the number of accessible Brønsted acid sites was performed by adsorption of ammonia at room temperature. After the ammonia loading, the samples were evacuated at 453 K for 2 h to eliminate physisorbed ammonia. Quantitative ^{1}H MAS NMR measurements were performed by comparing the signal intensities of the samples under study with the intensity of an external intensity standard (dehydrated zeolite H,Na-Y with the cation exchange degree of 35%). The decomposition and simulation of NMR spectra were carried out via the Bruker software WINFIT.

^{1}H PFG NMR investigations of the self-diffusivity of ethane and ethylene in SAPO-34 were performed using a Bruker Diff-30 diffusion probe with a 5 mm NMR coil insert and a z-gradient unit with a 40 A amplifier. Via a three-pulse echo sequence, the NMR self-diffusion was obtained by recording a series of ^{1}H NMR echoes with increasing magnetic field gradient strength up to g = 1200 G/cm. The calibration of the strength of the magnetic field gradients was performed via the self-diffusion coefficient of liquid water at 298 K.

For the ^{1}H PFG NMR experiments performed at 295 K, a diffusion time of Δ = 40 ms was used. The variable-temperature (T = 303−353 K) ^{1}H PFG NMR experiments were carried out with diffusion times of Δ = 10−40 ms. Under these conditions, no unwanted signals of surface sites or occluded organic deposits were observed in the echoes. The PFG NMR self-diffusivity coefficients, D, were calculated using the Bruker BioSpin software Diffusion Version 003. With this software, the decay of the echo intensities, $I(g)/I(0)$, as a function of the squared gradient strength, g^2, for constant gradient pulse duration and diffusion time was fitted to obtain the self-diffusion coefficients, D.[24]

Upon transferring the catalyst samples used for the PFG NMR investigations from the fixed-bed reactor into the 5 mm glass tubes, ethane and ethene (both 99.95 vol. %, Westfalen AG, Germany) were quantitatively adsorbed using a vacuum line after evacuation of the samples at 293 K for 1 h. The adsorbate concentration on the MTO catalysts was controlled by evaluating the signal intensities of single-pulse ^{1}H NMR spectra of the samples used for the self-diffusion studies.

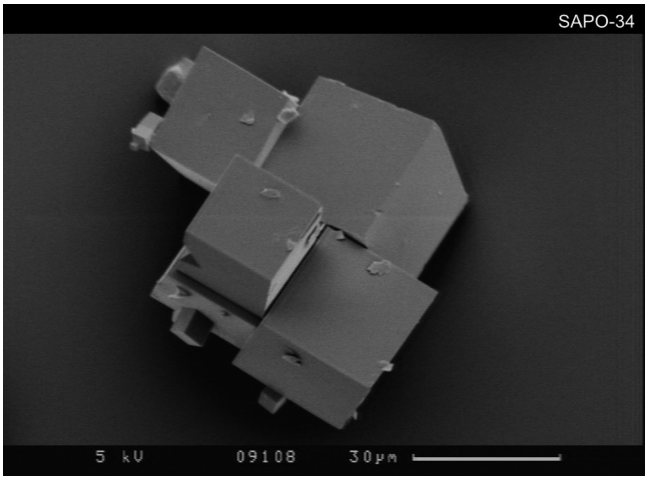

Figure 1. SEM image of large-crystalline SAPO-34.

3. RESULTS AND DISCUSSION

3.1. Physicochemical Properties of Large-Crystalline SAPO-34. The SEM image in Figure 1 shows the crystal morphology of the as-synthesized large-crystalline SAPO-34. The SAPO-34 crystals appear as cubes with sizes of 20−30 μm. Only few significantly smaller crystals occurred with a size of ca. 5 μm. The XRD pattern (not shown) agreed well with those of SAPO-34 materials described in the literature.[19,29] The surface area of the calcined sample was determined to 471 m^2/g, indicating the intactness and accessibility of the pore system.

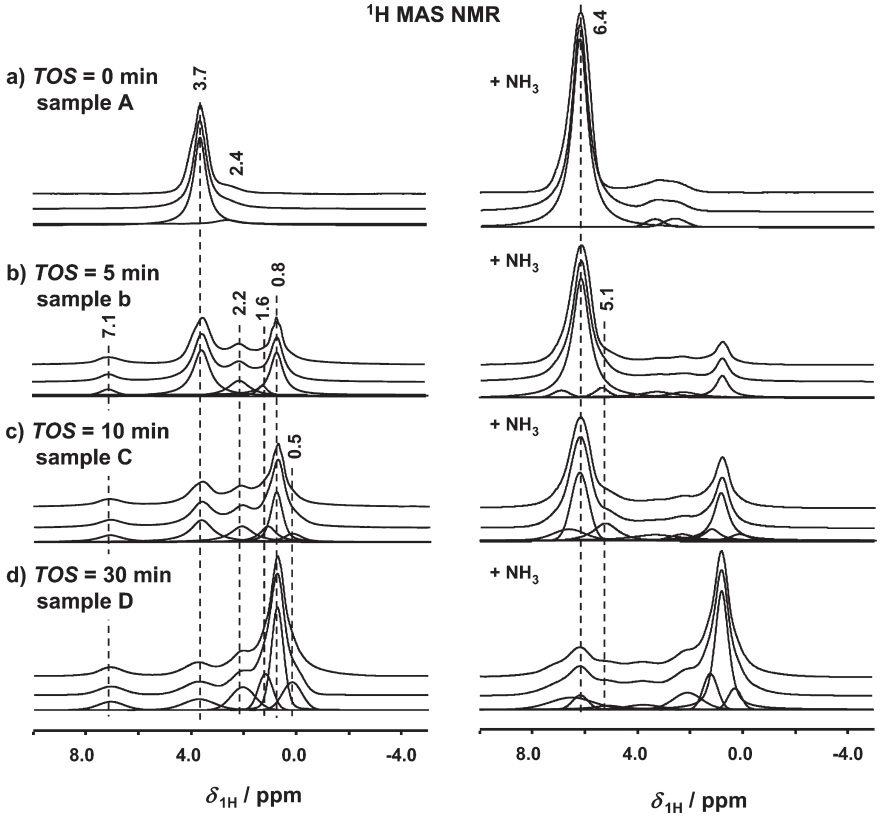

Figure 2. ^{1}H MAS NMR spectra of large-crystalline SAPO-34 after MTO conversion with time-on-stream of TOS = 0 min (sample A) to 30 min (sample D) recorded before (left) and after (right) adsorption of ammonia.

dx.doi.org/10.1021/jp208815g |J. Phys. Chem. C 2012, 116, 2469–2476

Table 1. Numbers of Accessible Bridging OH Groups (SiOHAl), n_{SiOHAl}, and Benzene-Based Carbenium Ions, $n_{benzenium}$, on Large-Crystalline SAPO-34 Used as MTO Catalyst for Different Times on Stream (TOS = 0−30 min)[a]

catalyst	TOS (min)	n_{SiOHAl}[b] (mmol g^{-1})	$n_{benzenium}$[b] (mmol g^{-1})
sample A	0	0.91	0
sample B	5	0.54	0.08
sample C	10	0.31	0.12
sample D	30	0.05	0.01

[a] These numbers were determined by quantitative ^{1}H MAS NMR spectroscopy after ammonia adsorption. [b] Experimental accuracy of ±5%.

^{29}Si MAS NMR spectroscopy (not shown) was utilized to investigate the nature of silicon in the large-crystalline SAPO-34. Only very weak signal intensities occurred at −100 to −115 ppm, hinting to a very small content of siliceous islands Si(4Si). The significantly stronger ^{29}Si MAS NMR signal with maximum at −89 ppm indicated a nearly complete incorporation of silicon into Si(4Al) sites by substitution of framework phosphorus atoms. This substitution route is accompanied by the formation of negative framework charges, which are compensated by Brønsted acidic bridging OH groups (SiOHAl).[30] The concentration of these Brønsted acid sites was determined by quantitative ^{1}H MAS NMR spectroscopy. Figure 2a shows the spectra of the dehydrated large-crystalline SAPO-34 before application as MTO catalyst (nonused sample A). The spectrum on the left-hand side consists of signals at 3.7 ppm due to bridging OH groups and at ca. 2.4 ppm caused by SiOH, AlOH, and POH groups.[31] Upon adsorption of ammonia, ammonium ions are formed at the accessible bridging OH groups, which leads to the signal at 6.4 ppm in Figure 1a, right.[31] Evaluation of the intensity of the ammonium signal at 6.4 ppm gives the number of accessible Brønsted acid sites, which is 0.91 mmol SiOHAl/g for the nonused SAPO-34 sample A (see Table 1, column 3).

3.2. Catalytic Performance of Large-Crystalline SAPO-34. The time dependence of the methanol conversion and product selectivity during the MTO conversion over the large-crystalline SAPO-34 is shown in Figure 3. In former studies on MTO conversion over small-crystalline SAPO-34 with particle sizes of 3−5 μm, a methanol conversion of 100% and a selectivity to light olefins of up to 85% were reached at 673 K for a time-on-stream up to TOS = 10 h.[18] For the large-crystalline SAPO-34 in the present study, rapid deactivation required a decrease of the reaction temperature to 643 K. Under these conditions, a drop-down of the methanol conversion from 100% at TOS = 5 min to 38% at TOS = 30 min was observed (Figure 3). At the same time, the selectivity to light olefins decreased from 91% to 5%. Hence, while the activity of large-crystalline SAPO-34 at TOS = 5 min is slightly higher (lower reaction temperature and higher olefin selectivity) in comparison with small-crystalline SAPO-34 in earlier studies, the significant larger particle size of the former catalyst causes a much stronger deactivation. This rapid deactivation may be due to organic deposits leading to a blocking of cages or pores.

For quantifying these organic deposits formed on large-crystalline SAPO-34 after MTO conversion times of TOS = 5, 10, and 30 min, the weight loss of the catalyst samples B, C, and D, respectively, were determined by TGA under flowing synthetic air in the temperature range of 293−1073 K. According to Figure 4, all samples show a similar low-temperature weight loss of ca. 2% up to 573 K due to volatile compounds. In the high-temperature

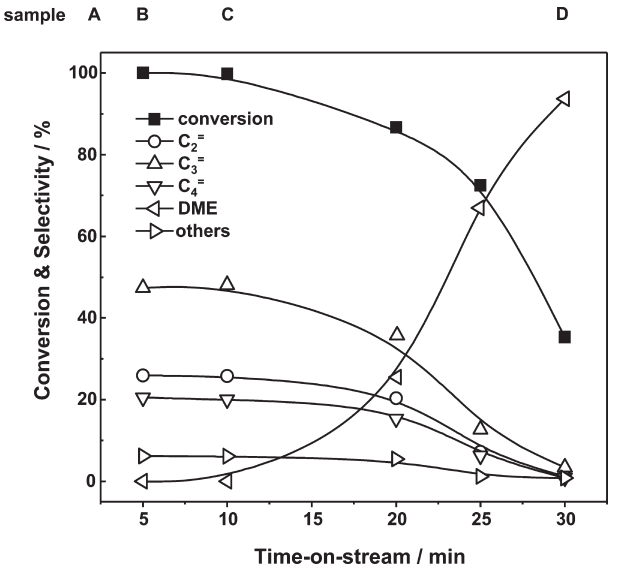

Figure 3. Methanol conversion and product selectivity over large-crystalline SAPO-34 at 643 K up to the time-on-stream of TOS = 30 min. On top, the time-on-stream for taking the catalyst samples A to D is marked.

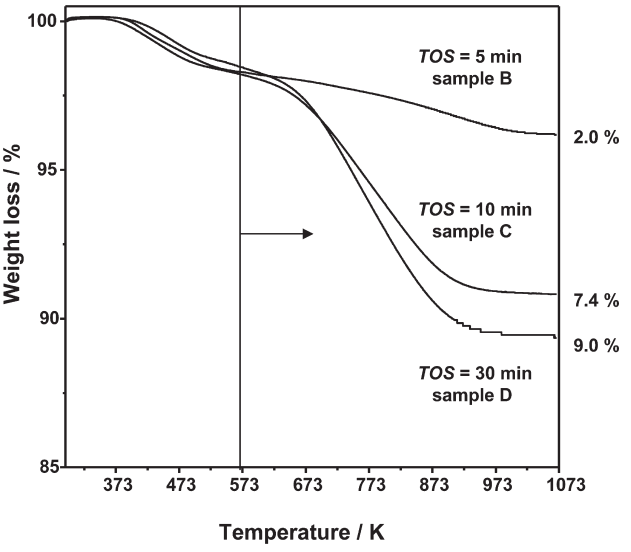

Figure 4. TGA curves of large-crystalline SAPO-34 determined after MTO conversion with time-on-stream of TOS = 5 min (sample B) to 30 min (sample D).

range of 573−1073 K, a weight loss of up to 9.0% for the deactivated catalyst sample D (TOS = 30 min) was determined. Interestingly, this weight loss is only 1.6% larger than the weight loss of the highly active SAPO-34 sample C obtained after TOS = 10 min. This finding indicates that only few coke deposits are required to cause a significant deactivation of large-crystalline SAPO-34.

3.3. In Situ UV/vis and ^{13}C MAS NMR Studies of Organic Deposits Formed during MTO Conversion on Large-Crystalline SAPO-34. For studying the nature of olefinic and aromatic compounds formed during the MTO conversion, in situ UV/vis spectroscopy was performed using a fiber-optic installed on top of the fixed-bed reactor.[32] The in situ UV/vis spectra in Figure 5

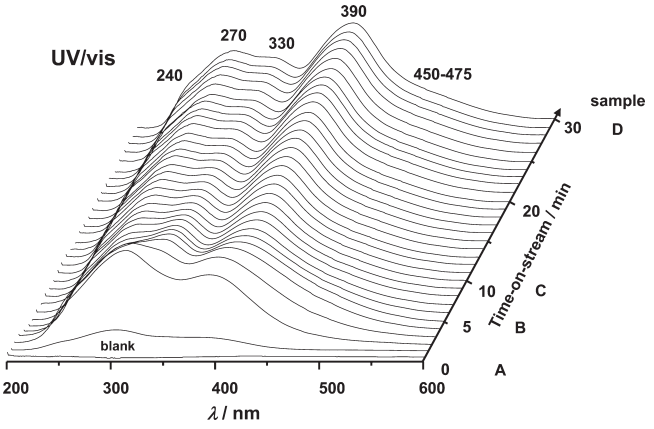

Figure 5. In situ UV/vis spectra recorded during MTO reaction on large-crystalline SAPO-34. On the right-hand side, the time-on-stream of the catalyst samples A to D is marked.

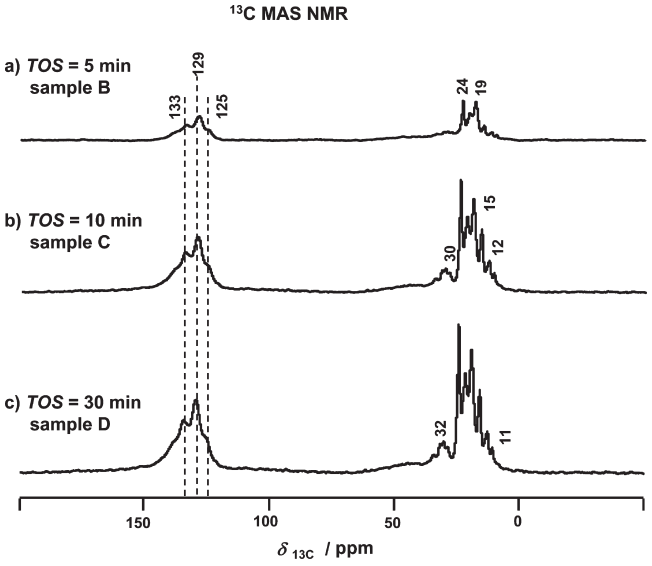

Figure 6. ^{13}C MAS NMR spectra of large-crystalline SAPO-34 recorded after MTO conversion with time-on-stream of TOS = 5 min (sample B) to 30 min (sample D).

show a rapid increase of bands at 240, 270, and 390 nm in the first 5 min of the MTO reaction. This duration corresponds to the induction period of the MTO reaction leading to the formation of first hydrocarbons. For longer MTO reaction times (TOS > 5 min), additional broad bands occur at 330 and 450−475 nm. Based on earlier UV/vis studies of organic compounds on acidic zeolite catalysts,[18,19,32−34] the bands at 240 and 270 nm were assigned to UV/vis sensitive dienes and polyalkylaromatics, while the band at 390 nm is explained by benzene-type carbenium ions. Often, broad bands at 330 and 450−475 nm are a hint for the presence of dienylic and trienylic carbenium ions, respectively. On the other hand, these UV/vis bands can be also explained by polycyclic aromatics.

The ^{13}C MAS NMR spectra in Figure 6 consist of characteristic signals in the range of polyalkylaromatics of 125−137 ppm.[35] Signals at 126, 129, and 133 ppm accompanied by signals at 19−21 ppm indicate the formation of polymethylbenzenes with different numbers of methyl groups. Signals at 25−32 ppm are a hint for ethyl groups bound to aromatic rings.[35] It should be mentioned that also polycyclic aromatics, such as naphthene, anthracene, and pyrene, may cause ^{13}C MAS NMR signals with typical relative intensities in the chemical shift range of 125−133 ppm.[35] However, the relative intensities of the ^{13}C MAS NMR signals at 125−137 and 19−32 ppm of the MTO catalyst obtained after TOS = 30 min (sample D) agree very well with those of samples B and C (TOS = 5 and 10 min, respectively). Therefore, a significant formation of polycyclic aromatic compounds on the SAPO-34 sample D can be excluded, since a large content of these compounds would cause additional characteristic signals, which were not observed in the ^{13}C MAS NMR spectrum of this MTO catalyst (sample D). This finding agrees very well with the small difference of 1.6 wt % in the weight loss of samples C and D as determined by TGA after MTO catalysis (vide supra).

3.4. ^{1}H MAS NMR Studies of the Fate of Surface Sites during the MTO Reaction. Quantitative evaluation of the ^{1}H MAS NMR spectra of large-crystalline SAPO-34 recorded after loading with ammonia give the number of accessible Brønsted acid sites and benzene-based carbenium ions existing on the MTO catalysts after TOS = 0−30 min (Figure 2 and Table 1, columns 3 and 4). After adsorption of ammonia on the catalyst samples, bridging OH groups responsible for ^{1}H MAS NMR signals at 3.7 ppm are transformed into ammonium ions causing signals at 6.4 ppm. In the presence of benzene-based carbenium ions, additional signals occur at 5.1 ppm due to the formation of phenylammonium ions.[18] Quantitative ^{1}H MAS NMR spectroscopy of the above-mentioned ammoniated species has the advantage of evaluating exclusively signals of accessible surface species.

The densities of accessible Brønsted acid sites are interesting for the correlation with the catalytic property of the SAPO-34 materials under study. According to Figure 2 and Table 1, column 3, a rapid decrease of the density of accessible bridging OH groups by 40% (comparison of samples A and B) occurs after TOS = 5 min of the MTO conversion on large-crystalline SAPO-34. After TOS = 10 min, an additional 25% of the accessible bridging OH groups are lost (comparison of samples B and C), which has, however, no significant influence on the MTO activity as shown in Figure 3. This indicates that only few Brønsted acid sites are required for highly active SAPO-34 catalysts in the MTO conversion. At the same time (TOS = 5 min), a significant number (0.12 mmol/g) of benzene-based carbenium ions were detected, which may play a role as catalytically active hydrocarbon pool compounds (Table 1, column 4). On the other hand, after TOS = 30 min (sample D), the density of accessible bridging OH groups dropped down to ca. 5% of the initial value, which agrees well with the strong decrease of the MTO activity (see Figure 3). This strong decrease of the density of accessible bridging OH groups indicates their covering or blocking by hydrocarbons and coke compounds.

3.5. PFG NMR Self-Diffusion Studies of Ethane and Ethene in Large-Crystalline SAPO-34 after Different MTO Conversion Times. Ethane is an often used molecule for studying PFG NMR self-diffusion in microporous materials (see refs 24, 26, 36, and 37 and references therein). In zeolites with 10-ring pores, such as in MFI-type zeolites, also the self-diffusivities of propane and propene were determined, but there is a strong limitation for PFG NMR self-diffusion studies of these molecules in 8-ring zeolites.[24,26,36] In a siliceous zeolite A (Si-LTA), Hedin et al.[26] determined a PFG NMR self-diffusivity of propene of $D = 4.7 \times 10^{-15}$ m^2 s^{-1}, which is about 4 orders of magnitude smaller in comparison with the self-diffusivity of ethene of $D = 2.1 \times 10^{-11}$ m^2 s^{-1} determined under same

dx.doi.org/10.1021/jp208815g |J. Phys. Chem. C 2012, 116, 2469–2476

Table 2. PFG NMR Self-Diffusion Coefficients, *D*, of Ethene and Ethane Loaded on Large-Crystalline SAPO-34 Used as MTO Catalyst for Different Times on Stream of TOS = 0 (Sample A) to 30 min (Sample D) Determined at 295 K

	$D/m^2\ s^{-1}$			
loading/cage	sample A TOS = 0 min	sample B TOS = 5 min	sample C TOS = 10 min	sample D TOS = 30 min
1 ethene	1.3×10^{-11}	8.0×10^{-12}	7.7×10^{-12}	5.8×10^{-12}
1 ethane	6.7×10^{-12}	4.9×10^{-12}	2.4×10^{-12}	2.2×10^{-12}
2 ethene	1.3×10^{-11}	9.2×10^{-12}	8.7×10^{-12}	*a*
2 ethane	5.7×10^{-12}	4.4×10^{-12}	2.3×10^{-12}	*a*
3 ethene	1.6×10^{-11}	1.1×10^{-11}	9.9×10^{-12}	*a*
3 ethane	4.4×10^{-12}	4.1×10^{-12}	2.3×10^{-12}	*a*

[a] These loadings of ethene and ethane could not be performed because of the decreased adsorption capacity of the deactivated sample D (TOS = 30 min).

conditions (T = 301 K). For a siliceous chabazite (Si-CHA), these authors obtained a self-diffusivity of ethene of $D = 3.1 \times 10^{-12}$ $m^2\ s^{-1}$, which is about 1 order of magnitudes smaller than in siliceous zeolite A (Si-LTA).[26] Based on these data, a self-diffusivity of propene in CHA-type zeolites in the order of 10^{-16} m^2/s has to be expected, which is not available for the experimental technique used in the present work. Therefore, the present study focused on the investigation of the smaller C_2-hydrocarbons ethane and ethene in large-crystalline SAPO-34, also because ethene is one of the most important reaction products of the methanol-to-olefin conversion on this catalyst material.

Table 2 gives a survey on the PFG NMR self-diffusivities of ethene and ethane in large-crystalline SAPO-34 for loadings of 1−3 molecules per chabazite cage and determined at 295 K. Considering the diffusivities of ethane in the nonused SAPO-34 sample A (TOS = 0 min), self-diffusivities of $D = 6.7 \times 10^{-12}$−4.4×10^{-12} $m^2\ s^{-1}$ for loadings of 1−3 molecules per cage were determined. These values as well as their variation with increasing adsorbate loading are in reasonable agreement with literature.[23,36] For the SAPO-34 samples obtained after TOS = 0−30 min and upon loading of 1 adsorbate molecule per cage, the systematic decrease of the self-diffusivity, D, of ethane with increasing MTO conversion time indicates a growing hindrance of molecular diffusion by organic deposits. A similar observation was made for the ethene self-diffusivity in the SAPO-34 samples obtained after TOS = 0−30 min.

Comparing the absolute self-diffusivities of ethene and ethane under same conditions (same TOS values and adsorbate loadings), significant higher D values were determined for ethene than for ethane. Similarly, in a very recent PFG MAS NMR study of self-diffusivities of ethene and ethane in the microporous metal−organic framework ZIF-8, a diffusion selectivity of $D_{ethene}/D_{ethane} = 5.5$ was found.[37] In the present study of ethene and ethane self-diffusivities in large-crystalline SAPO-34, this diffusion selectivity increases from $D_{ethene}/D_{ethane} = 1.9$ for sample A (TOS = 0 min) loaded with 1 molecule per cage to $D_{ethene}/D_{ethane} = 3.6$ upon loading with three molecules. Hence, with increasing adsorbate concentration, the diffusion selectivity changes to the benefit of the smaller olefin.

Very interestingly, there is also a change of the diffusion selectivity for ethene and ethane with increasing MTO reaction time. Comparing the catalytically active SAPO-34 samples A (TOS = 0 min) to C (TOS = 10 min), the diffusion selectivity increases from $D_{ethene}/D_{ethane} = 1.9$ to $D_{ethene}/D_{ethane} = 3.2$ for an adsorbate loading of the catalyst with 1 molecule per cage and from $D_{ethene}/D_{ethane} = 2.3$ to $D_{ethene}/D_{ethane} = 3.8$ for an adsorbate loading with 2 molecules per cage. Hence, also for increasing MTO reaction time, the diffusion selectivity changes to the benefit of the smaller olefin in comparison with the larger alkane. This finding indicates that the hydrocarbon pool compounds formed during the active lifetime of SAPO-34 used as MTO catalyst lead to a change of the effective pore diameter, which influences the self-diffusion of adsorbate molecules with different sizes in a different manner. First for the deactivated SAPO-34 sample D (TOS = 30 min), a total blocking of a significant content of pores occurs, as indicated by the strong dropdown of the density of the accessible acid sites (Table 1, column 3) and the strong decrease of the adsorption capacity (see footnote of Table 2). For the remaining accessible pores of the deactivated SAPO-34 sample D (TOS = 30 min), however, self-diffusivities of ethene and ethane with only slightly lower D values were determined than for the SAPO-34 samples A to C after TOS ≤ 10 min (Table 2, column 5).

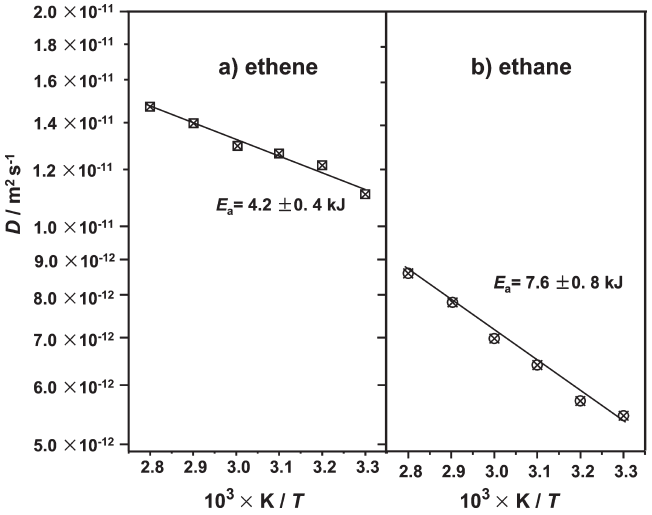

Figure 7. Arrhenius plots of the PFG NMR self-diffusivities, D, of ethene (a) and ethane (b) on large-crystalline SAPO-34 sample A (TOS = 0 min) loaded with 2 molecules per cage and determined in the temperature range of 303−353 K.

Initiated by the above-mentioned observation of the diffusion selectivity for ethene and ethane in SAPO-34, the apparent activation energies, E_a, for the self-diffusion of these molecules were investigated in the temperature range of 303−353 K. At these temperatures, a chemical conversion of ethene over SAPO-34 can excluded. In Figure 7a,b, the Arrhenius plots, $D = D_0 \exp\{-(E_a/kT)\}$, of the PFG NMR self-diffusivities D of ethene

dx.doi.org/10.1021/jp208815g |J. Phys. Chem. C 2012, 116, 2469–2476

and ethane as a function of the inverse temperature T are shown. These D values were obtained for an adsorbate loading of the large-crystalline SAPO-34 sample A (TOS = 0 min) with 2 molecules per cage. Evaluation of the slopes of the Arrhenius plots gave apparent activation energies of E_a = 4.2 kJ/mol and E_a = 7.6 kJ/mol for the self-diffusion of ethene and ethane, respectively. Similarly, for the self-diffusion of ethene and ethane in the metal−organic framework ZIF-8,[37] apparent activation energies of E_a = 4.9−6.6 kJ/mol and E_a = 8.6−9.6 kJ/mol, respectively, were determined for loadings of ZIF-8 differing by a factor of 2.

4. CONCLUSIONS

A large-crystalline SAPO-34 catalyst with particle sizes of 20−30 μm was prepared and used for first studies of ethene and ethane self-diffusivities in MTO (methanol-to-olefin) catalysts after different methanol conversion times. Simultaneously with the catalytic investigations, in situ UV/vis spectroscopic studies of organic compounds formed during the MTO conversion over SAPO-34 were carried out. After TOS = 0−30 min of the MTO reaction, catalyst samples were taken from the fixed-bed reactor for detailed solid-state NMR studies of organic deposits and active surface sites. Furthermore, the catalyst samples obtained after MTO conversion times of TOS = 0−30 min were utilized for PFG NMR investigations of the self-diffusivities of ethane and ethene.

Comparing the performance of the large-crystalline SAPO-34 catalyst in the MTO reaction with that of small-crystalline SAPO-34 catalysts in the literature, a significant shortening of the catalysts lifetime was found due to the large particle size and, therefore, long pores. On the other hand, typical organic deposits were formed on the working large-crystalline SAPO-34 catalysts, such as polymethylaromatics being the catalytically active hydrocarbon pool compounds of the MTO reaction. The formation of a large content of polycyclic aromatics acting as coke deposits on the deactivated MTO catalyst could be excluded by ^{13}C MAS NMR spectroscopy. Hence, only few organic deposits cause a reasonable blocking of pores in large-crystalline SAPO-34, making this material inactive after a MTO conversion time of TOS = 30 min. This finding agrees with the strong decrease of accessible Brønsted acid sites determined by ^{1}H MAS NMR spectroscopy for the deactivated SAPO-34 catalyst obtained after TOS = 30 min.

In the PFG NMR self-diffusion studies on large-crystalline SAPO-34, a systematic decrease of the self-diffusivity, D, of ethene and ethane with increasing MTO reaction time was found. This observation indicates a growing hindrance of molecular diffusion by organic deposits, which do not block the pores in a total manner but modify the effective pore diameters and cage sizes. These organic deposits are probably hydrocarbon pool compounds, such as polymethylaromatics contributing to the MTO conversion, and not polycyclic aromatics leading to a total blocking of the SAPO-34 cages and pores.

Using the ratio of the self-diffusivities of ethene and ethane, D_{ethene}/D_{ethane}, as a measure of the diffusion selectivity of these adsorbate molecules, an increase of the diffusion selectivity toward the smaller olefin in comparison with the larger alkane was found, if the adsorbate loading of nonused and used SAPO-34 catalysts becomes higher. Similarly, an increase of the diffusion selectivity to the benefit of the smaller olefin was observed with increasing MTO reaction time. This change of the diffusion selectivity of SAPO-34 during the MTO reaction may be one of the reasons for the variation of the product selectivity of this catalyst during its lifetime. In agreement with the experimentally observed diffusion selectivity of ethene and ethane in SAPO-34 catalysts toward to smaller olefin, a significantly larger apparent activation energy for the self-diffusion of ethane than for ethene was determined.

AUTHOR INFORMATION

Corresponding Author

*Fax +49-711-685-64081, e-mail michael.hunger@itc.uni-stuttgart.de (M.H.); Fax +86-22-2350-0341, e-mail lild@nankai.edu.cn (L.L.).

ACKNOWLEDGMENT

This work was supported by the National Basic Research Program of China (2009CB623502) and MOE (IRT0927). Furthermore, M.H. thanks the Fonds der Chemischen Industrie and Deutsche Forschungsgemeinschaft for financial support.

REFERENCES

(1) Kvisle, S.; Fuglerud, T.; Kolboe, S.; Olsbye, U.; Lillerud, K.-P.; Vora, B. V. Methanol-to-Hydrocarbons. In *Handbook of Heterogeneous Catalysis*, 2nd ed.; Ertl, G., Knözinger, H., Schüth, F., Weitkamp, J., Eds.; Wiley-VCH: Weinheim, 2008; Vol. 6, pp 2950−2964.

(2) Stöcker, M. Methanol to Olefins (MTO) and Methanol to Gasoline (MTG). In *Zeolites and Catalysis*; Cejka, J., Corma, A., Zones, S., Eds.; Wiley-VCH: Weinheim, 2010; pp 687−711.

(3) Haw, J. F.; Song, W.; Marcus, D. M.; Nicholas, J. B. *Acc. Chem. Res.* **2003**, *36*, 317–326.

(4) Olsbye, U.; Bjørgen, M.; Svelle, S.; Lillerud, K. P.; Kolboe, S. *Catal. Today* **2005**, *106*, 108–111.

(5) Karge, H. G.; Weitkamp, J. *Molecular Sieves, Adsorption and Diffusion*; Springer-Verlag: Berlin, 2008; Vol. 7.

(6) Weitkamp, J.; Ernst, S.; Puppe, L. Shape-Selective Catalysis in Zeolites. In *Catalysis and Zeolites*; Weitkamp, J., Puppe, L., Eds.; Springer-Verlag: Berlin, 1999; pp 327−376.

(7) Chang, C. D. *Catal. Rev.—Sci. Eng.* **1984**, *26*, 323–345.

(8) Stöcker, M. *Microporous Mesoporous Mater.* **1999**, *29*, 3–48.

(9) Wilson, S.; Barger, P. *Microporous Mesoporous Mater.* **1999**, *29*, 117–126.

(10) Dahl, I. M.; Kolboe, S. *J. Catal.* **1994**, *149*, 304–309.

(11) Dahl, I. M.; Kolboe, S. *J. Catal.* **1996**, *161*, 458–464.

(12) Chen, D.; Rebo, H. P.; Moljord, K.; Holmen, A. *Ind. Eng. Chem. Res.* **1999**, *38*, 4241–4249.

(13) Song, W.; Haw, J. F.; Nicholas, J. B.; Heneghan, C. S. *J. Am. Chem. Soc.* **2000**, *122*, 10726–10727.

(14) Song, W.; Fu, H.; Haw, J. F. *J. Am. Chem. Soc.* **2001**, *123*, 4749–4754.

(15) Wu, X.; Abraha, M. G.; Anthony, R. G. *Appl. Catal., A* **2004**, *260*, 63–69.

(16) Hereijgers, B. P. C.; Bleken, F.; Nilsen, M. H.; Svelle, S.; Lillerud, K.-P.; Bjøgen, M.; Weckhuysen, B. M.; Olsbye, U. *J. Catal.* **2009**, *264*, 77–87.

(17) Bleken, F.; Bjørgen, M.; Palumbo, L.; Bordiga, S.; Svelle, S.; Lillerud, K.-P.; Olsbye, U. *Top. Catal.* **2009**, *52*, 218–228.

(18) Dai, W.; Scheibe, M.; Guan, N.; Li, L.; Hunger, M. *ChemCatChem* **2011**, *3*, 1130–1133.

(19) Dai, W.; Wang, X.; Wu, G.; Guan, N.; Hunger, M.; Li, L. *ACS Catal.* **2011**, *1*, 292–299.

(20) Karge, H. G.; Niessen, W. *Catal. Today* **1991**, *8*, 451.

(21) Jobic, H.; Methivier, A.; Ehlers, G.; Farago, B.; Haeussler, W. *Angew. Chem., Int. Ed.* **2004**, *43*, 364–366.

(22) Kirst, K. U.; Kremer, F.; Litvinov, V. M. *Macromolecules* **1993**, *26*, 975.

(23) Kärger, J.; Ruthven, D. M. *Diffusion in Zeolites and Other Microporous Solids*; Wiley: New York, 1992.
(24) Kärger, J. Diffusion Measurements by NMR Techniques. In *Molecular Sieves, Adsorption and Diffusion*; Karge, H. G., Weitkamp, J., Eds.; Springer-Verlag: Berlin, 2008; Vol. 7, pp 85−133.
(25) Bär, N.-K.; Kärger, J.; Pfeifer, H.; Schäfer, H.; Schmitz, W. *Microporous Mesoporous Mater.* **1998**, *22*, 289–295.
(26) Hedin, N.; DeMartin, G. J.; Roth, W. J.; Strohmaier, K. G.; Reyes, S. C. *Microporous Mesoporous Mater.* **2008**, *109*, 327–334.
(27) Einstein, A. *Investigations on the Theory of Brownian Movement*; Dover Publications: Mineola, NY, 1926; p 119.
(28) Iwase, Y.; Motokura, K.; Koyama, T.; Miyaji, A.; Baba, T. *Phys. Chem. Chem. Phys.* **2009**, *11*, 9268–9277.
(29) Treacy, M. M. J.; Higgins, J. B. *Collection of Simulated XRD Powder Patterns for Zeolites*, 5th Revised Ed.; Elsevier: Amsterdam, 2007; p 115.
(30) Zibrowius, B.; Löffler, E.; Hunger, M. *Zeolites* **1992**, *12*, 167–174.
(31) Jiang, Y.; Huang, J.; Dai, W.; Hunger, M. *Solid State Nucl. Magn. Reson.* **2011**, *39*, 116–141.
(32) Jiang, Y.; Huang, J.; Weitkamp, J.; Hunger, M. *Stud. Surf. Sci. Catal.* **2007**, *170*, 1137–1144.
(33) Kirisci, I.; Førster, H.; Tasi, G.; Nagy, J. B. *Chem. Rev.* **1999**, *99*, 2085–2114.
(34) Bjørgen, M.; Bonino, F.; Kolboe, S.; Lillerud, K.-P.; Zecchina, A.; Bordiga, S. *J. Am. Chem. Soc.* **2003**, *125*, 15863–15868.
(35) Kalinowski, H.-O.; Berger, S.; Braun, S. *^{13}C NMR Spektroskopie*; Thieme Verlag: Stuttgart, 1984; pp 134−142.
(36) Caro, J.; Bülow, M.; Schirmer, W.; Kärger, J.; Heink, W.; Pfeifer, H.; Zdanov, S. P. *J. Chem. Soc., Faraday Trans. 1* **1985**, *81*, 2541–2550.
(37) Chmelik, C.; Freude, D.; Bux, H.; Haase, J. *Microporous Mesoporous Mater.* **2011**, *147*, 135–141.